Available online at www.HEFJournal.org

ISSN: 2785-2997

Journal of
Human, Earth, and Future

Vol. 6, No. 4, December, 2025

Optimizing Piezoelectric Energy Harvesters: A Study on Magnetic Nonlinearity

Fahmidul Huq Syed [1], Li Wah Thong [1*], Mirza Farrukh Baig [2], Yee Kit Chan [1], M. N. Ervina Efzan [1, 2]

[1] *Faculty of Engineering and Technology, Multimedia University, Bukit Beruang, 75450 Malacca, Malaysia.*

[2] *Centre for Manufacturing and Environmental Sustainability, Multimedia University, Bukit Beruang, 75450 Malacca, Malaysia.*

Received 22 July 2025; Revised 17 November 2025; Accepted 22 November 2025; Published 01 December 2025

Abstract

This study aims to optimize the performance of piezoelectric energy harvesters (PEHs) by comparing linear and nonlinear configurations, with a focus on the role of magnetic nonlinearity. The objective is to address the limitations of conventional linear PEHs, which typically suffer from narrow bandwidth and limited power output, by exploring the integration of repulsive permanent magnets to induce nonlinear behavior. Analytical modelling combined with finite element analysis (FEA) was employed to evaluate voltage generation, power output, and resonant frequency in both models under consistent geometrical parameters. The linear configuration, featuring a single tip mass, achieved a peak output of 2.63 V and 0.29 mW at 111 Hz, aligning closely with validated analytical and FEA predictions. In contrast, the nonlinear model incorporating permanent magnets exhibited two distinct peaks, with a maximum output of 7.83 V and 1.92 mW at 74 Hz, results that were consistent with experimental validation despite minor frequency deviations. The findings highlight that nonlinear magnetic coupling significantly improves energy harvesting efficiency and broadens operational bandwidth compared to linear systems. The novelty of this study lies in its comprehensive comparison of magnet-integrated nonlinear PEHs against conventional designs, offering valuable insights for developing efficient, broadband, and sustainable energy harvesting technologies.

Keywords: Piezoelectric Energy Harvesters; Vibration Energy, Broadband Frequency; Cantilever Beam; Nonlinear Dynamics.

1. Introduction

Imagine a world where the vibrations of daily life fuel our devices, eliminating the need for batteries and reducing our reliance on centralized energy sources. This vision is encapsulated in the potential of piezoelectric energy harvesters (PEH), compact devices capable of transforming mechanical energy derived from vibrations, pressure, or sound into usable electrical energy [1]. This technology holds immense potential for powering low-power electronics, wireless sensor networks, and even medical implants, offering a sustainable and self-sufficient alternative to traditional power sources [2].

At the heart of these harvesters lies the piezoelectric effect, a fascinating phenomenon exhibited by certain materials. When pressure or stress is applied to these materials, their internal crystal structure changes, causing an electric potential difference across their surfaces. This potential difference can be harnessed to generate a small electric

* Corresponding author: lwthong@mmu.edu.my

http://dx.doi.org/10.28991/HEF-2025-06-04-015

current. Conversely, applying an electric field to these materials can cause them to physically deform, proving the reversibility of the effect [3, 4]. PEHs come in various shapes and sizes but most commonly utilize cantilever beams made of piezoelectric materials like lead zirconate titanate (PZT) [5, 6]. These beams are designed to resonate at specific frequencies, efficiently converting ambient vibrations into electrical energy. The generated voltage is typically low, but by incorporating circuits and energy storage elements like capacitors, harvesters can power small electronics or accumulate energy for later use [7].

PEH systems have been widely studied for their potential in addressing key supply problems in microelectronic devices. Traditional linear PEH typically harnesses energy solely from vibrations traveling in a single direction, leading to narrow resonance frequency bands and suboptimal energy conversion efficiency. In response, researchers have introduced diverse nonlinear PEH designs to address these constraints. Nonlinear PEH systems have been extensively studied in recent research [8–11]. Various approaches have been proposed to improve the performance of these systems. One approach is the use of a nonlinear energy sink combined with a piezoelectric energy harvester, which can achieve simultaneous vibration absorption and energy harvesting [12]. Researchers have proposed a novel device that combines an Euler-buckled beam nonlinear energy sink with a piezoelectric energy harvester, demonstrating that multi-objective optimization can improve vibration mitigation performance and increase energy harvesting capacity by over 60% compared to traditional linear vibration absorbers [13]. A new magnetically excited piezoelectric harvester with a nonlinear energy sink has also been proposed to expand bandwidth and increase frequency bands, successfully powering LEDs and Bluetooth sensors [14].

Additionally, a comparative study evaluated the energy harvesting performance of piezoelectric cantilever beams using three configurations—unimorph, bimorph, and stack—and two materials, PZT-5A and PVDF. The study found that PZT-5A significantly outperformed PVDF, with a voltage output up to 94% higher at resonance. Among the configurations, the bimorph beam with PZT-5A showed the highest energy conversion efficiency, increasing electrical power output by 50% compared to the unimorph configuration and 9% over the stack configuration. The research highlights the critical role of structural design and material properties in optimizing these devices for low-power applications [15]. Researchers examined a two-layer piezoelectric sensor featuring a non-linear single-mode configuration, aiming to uncover optimal conditions for power extraction [16]. Another approach involves the design of auxetic nonlinear energy harvesters with a clamped-clamped beam and multiple rotating square unit cells, which can provide a broad working bandwidth and high-power output [17]. Additionally, the use of a Duffing oscillator in piezoelectric energy harvesting systems has been investigated, and the bifurcation trees of period-1 motions to chaos have been obtained analytically [18]. Furthermore, the geometric nonlinearity of piezoelectric cantilever beams has been considered in the design of energy harvesters, leading to improved performance in terms of peak displacement and peak output power [19]. A wideband nonlinear beam-spring piezoelectric energy harvester has been proposed, which can harvest low-frequency wideband vibration energy [20]. An unconventional exact-tapered fixed-guided spring design was proposed to introduce nonlinearity into the system, resulting in enhanced bandwidth and power output. Moreover, a PEH modelled after a line tooth (PEH-ILT) was developed to capture three-dimensional stochastic vibrations, and its broadband conditions were determined through the Melnikov theory [21].

The optimization of parameters in nonlinear PEH systems for IoT applications has been investigated in several studies. The influence of different factors was investigated, including the distance between magnets, the addition of magnetic tip mass, and the placement of the vibrational source, on the frequency response output of a unimorph piezoelectric cantilever beam [22]. The numerical optimization of a mechanically and electrically nonlinear and nonideal PEH was also explored, considering different design variables and using a genetic algorithm [23]. An eco-friendly wind energy harvester was developed based on piezoelectric technology and optimized parameters such as piezoelectric thickness, wind speed, rotor angular velocity, and vibration enhancement mechanism stiffness [24]. In another study, the parameters of a DC-to-DC converter in a piezoelectric micro-energy harvesting system were optimized to maximize energy harvesting efficiency [25]. Response surface methodology was used to optimize parameters such as temperature, pressure, resistance, and frequency in a pre-stressed piezoelectric composite for energy harvesting [26]. In an experimental study, the parameter optimization of a magnetically coupled piezoelectric energy harvester was conducted, including magnet spacing and flux density, to increase output and bandwidth [27]. Additionally, a versatile non-linear model was developed to predict piezoelectric energy harvester performance. This model underwent validation through experimental testing, followed by a comparison of its results with those from a linear model. Through this process, researchers identified the dominant factors affecting piezoelectric harvester performance [28].

Broadband vibration energy harvesting can be improved through the utilization of a multimodal nonlinear magnetoelectric converter. The use of folded cantilevers and magnetic circuits allows for multi-resonant response and broadening of the frequency range [29]. A framework for analyzing a bistable PEH using the finite element method has been developed, with bistability achieved through magnetic interactions. Numerical simulations show that the nonlinear dynamics can be leveraged to improve energy harvesting performance across a wider frequency range [30]. Additionally, the adoption of three springs with equal intersection angles enables the absorption of multi-directional vibration energy, further enhancing the harvesting bandwidth [31]. Nonlinear techniques, such as introducing a magnetic field, can also be employed to broaden the operating bandwidth of PEH [32]. By integrating a duo of

magnets, a nonlinear 2-DOF PEH can attain a notably broader bandwidth compared to its linear equivalent [33]. Moreover, a proposed broadband vibration energy harvester, employing magnetoelectric transducers, leverages nonlinear magnetic force and multi-cantilever beams to extend the operational bandwidth [34]. Adjusting the angular orientation of external magnets further enhances the broadband frequency response of magnetically coupled nonlinear PEH.

A hybrid nonlinear approach is proposed to enhance the efficiency and widen the load bandwidth of piezoelectric energy scavenging. Combining two established techniques enables four energy extraction cycles per vibration period. Theoretical analysis and experimental findings demonstrate that this approach can harvest up to six times more energy, all while maintaining relative load independence [35]. Another study investigates the deliberate introduction of nonlinearities in a monostable piezoelectric harvester, which broadens the bandwidth and enables energy harvesting from low-frequency excitations. The study demonstrates the activation of superharmonic resonances and the extraction of considerable amounts of power at fractions of the natural frequency [36]. Additionally, an array of nonlinear piezomagnetoelastic energy harvesters is proposed, which combines the dynamic responses of monostable harvesters to achieve wide bandwidth and improved energy extraction under both harmonic and random excitations [37]. Another approach presents a wideband piezoelectric energy harvesting system based on a nonlinearly tapered harvester, which exhibits higher potential electromechanical outputs compared to traditional uniform harvesters [38]. Finally, a compact MEMS resonator design exploits the nonlinear stiffness of a doubly clamped beam to achieve ultra-wide-bandwidth energy harvesting with improved power density [39].

Analytical modeling, simulation, and experimental investigations have been carried out on the nonlinear hybrid piezoelectric-electromagnetic energy harvesting from stochastic excitation. The influence of nonlinear strength, load resistance, and excitation spectral density on the vibration response and electric output of the energy harvester has been examined. The study reveals that the mean power of the energy harvester exhibits a linear increase with acceleration spectral density [40]. Compared to a linear hybrid energy harvester, the resonant frequency of the nonlinear energy harvester can be reduced by 57%, while the output power can be augmented by 72% [41]. Under Gaussian white noise, the dynamics of the nonlinear electromechanical system demonstrate stochastic bifurcation [42]. Combining harmonic excitation with random force enhances the harvested energy. The hybrid model of the energy harvester shows better performance compared to piezoelectric and electromagnetic energy harvesters [43]. Maximizing the mean power and spectral density of the hybrid energy harvester hinges on determining the optimal load resistance for both the piezoelectric and electromagnetic elements. Nevertheless, the literature highlights that maximizing the efficiency and output power of PEHs remains a crucial challenge. While linear models with simple beam designs offer a straightforward approach, their output often falls short of practical requirements. Exploring alternative designs and configurations becomes paramount in pushing the boundaries of PEH technology.

While these developments demonstrate the promise of nonlinear approaches, critical gaps remain in the literature. First, many studies prioritize either numerical modeling or experimental prototypes, with limited efforts to systematically integrate analytical modeling, finite element analysis (FEA), and experimental validation. Second, the influence of magnetic parameters, such as spacing and flux density, is often studied alongside variations in beam geometry, making it difficult to isolate the precise role of magnetic nonlinearity [44]. Third, rigorous head-to-head comparisons of linear and nonlinear PEHs under identical geometric and material conditions are scarce, leaving an incomplete understanding of the performance trade-offs between conventional and magnetically integrated systems.

This study addresses these challenges by conducting a controlled performance comparison between two PEH configurations: a conventional linear model with a single tip mass and a nonlinear model incorporating repulsive permanent magnets. Analytical modeling is used to capture the system dynamics, including the cubic stiffness contributions from magnetic coupling. FEA simulations are then performed under consistent design parameters to quantify voltage, power, and resonance characteristics, followed by validation against experimental data. The results demonstrate that while the linear model achieves a peak voltage of 2.63 V and a power output of 0.29 mW at 111 Hz, the nonlinear model delivers significantly enhanced performance, producing 7.83 V and 1.92 mW at 74 Hz with two distinct resonance peaks.

The novelty of this work lies in its rigorous, side-by-side evaluation of linear and nonlinear PEHs under identical conditions, providing clarity on the role of magnetic coupling in enhancing bandwidth and energy efficiency. By integrating analytical, numerical, and experimental perspectives, this study advances the understanding of magnetically nonlinear harvesters and offers practical design insights for the development of efficient, broadband, and application-ready energy harvesting systems. The remainder of the paper is organized as follows: Section 2 introduces the analytical model of the linear and nonlinear PEHs, Section 3 outlines the finite element simulations, Section 4 describes the experimental setup for validation, Section 5 presents and discusses the comparative results, and Section 6 concludes with the key findings and directions for future work.

The methodology adopted in this study integrates analytical modelling and finite element analysis (FEA) to evaluate linear and nonlinear piezoelectric energy harvesters. The process begins with defining the two systems: a conventional cantilever with a tip mass and a magnetically coupled nonlinear variant. Analytical modelling establishes the equations of motion, stiffness terms, and electromechanical coupling, while accounting for magnetic nonlinearity. This is

followed by FEA, where the simulation domain is constructed using consistent material properties and system parameters. Key variables such as excitation frequency, load resistance, and magnet gap are systematically varied to assess their impact on performance. The complete methodological flow is summarized in Figure 1.

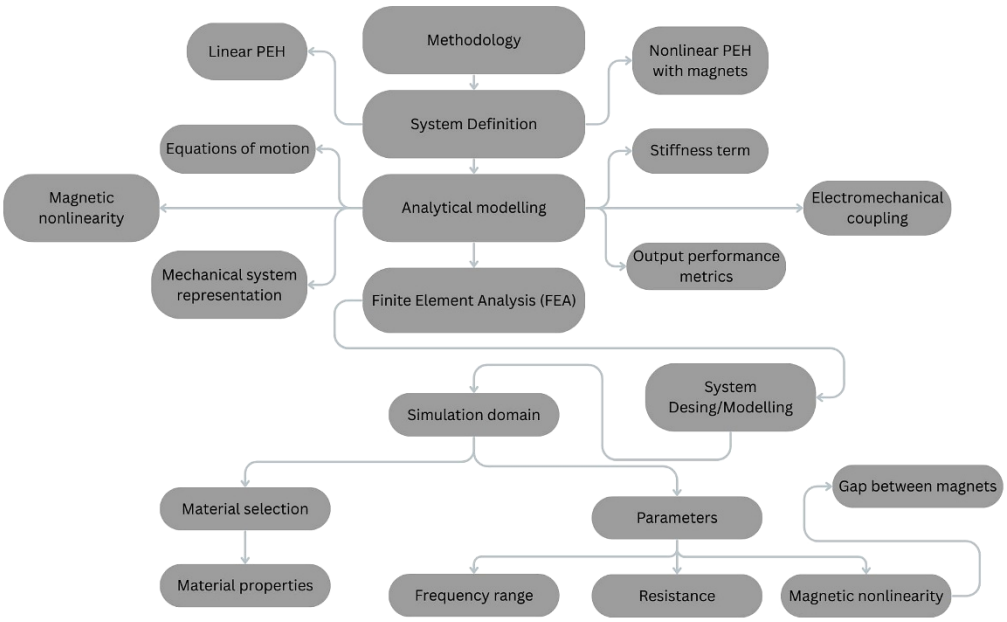

Figure 1. Workflow of the Methodology

2. Analytical Method

The analytical model consists of two models, a linear model with single mass block on the beam and a nonlinear model with two repulsive permanent magnets.

2.1. Linear Model

The analytical model of a single piezoelectric beam with a tip mass is presented. The Euler-Bernoulli equation of motion governing the behavior of the piezoelectric harvester is expressed as follows:

$$M\ddot{x}(t) + C\dot{x}(t) + Kx(t) - \theta v(t) = F(t) \tag{1}$$

$$C_p\dot{v}(t) + v(t)/R + \theta\dot{x}(t) = 0 \tag{2}$$

In this context, M represents the total mass, and C denotes damping, K and θ describe the effective stiffness and equivalent linear piezoelectric electromechanical coupling coefficient. C_p represents piezoelectric material capacitance, and $v(t)$ is the voltage across the external load resistance, R. Vertical displacement of the mass at the tip is denoted by $x(t)$, while $F(t)$ represents mechanically induced force by surrounding vibration excitation [45-47].

Since we are using a bimorph cantilever beam, the formula of capacitance can be modified by taking the presence of the substrate material into account,

$$C_p = 2\varepsilon_0 bL_p / h_p \tag{3}$$

where, ε_0 is the vacuum permittivity, and b signifies the width of cantilever beam. L_p denotes the length of piezoelectric layer, while h_p represents the thickness of the piezoelectric layer [48–50]. Since the substrate layers do not showcase any dielectric properties, hence they are not inclusive in the calculation of capacitance.

The formula for the voltage output can be given by,

$$V = g \cdot d_{31} \cdot \Delta p/\varepsilon_0 \cdot \varepsilon_r \cdot A_{eff} \tag{4}$$

where V represents voltage, g is the piezoelectric voltage constant, d_{31} denotes the piezoelectric strain constant, and Δp is the induced mechanical strain in the piezoelectric material due to external forces [51]. The formula for electrical output is as follows,

$$P = 0.5 \cdot C_p \cdot V^2 \cdot f \tag{5}$$

where, P represents the output electrical power (in milli watts), C_p is the capacitance of the piezoelectric energy harvester, V stands for the output voltage of the harvester and f is the frequency of mechanical excitation.

The analytical model has been implemented within the framework of FEA analysis to simulate the system and gather the resulting outputs. This process involved the use of advanced computational tools to accurately replicate the conditions and operations of the model, thereby facilitating a detailed examination of its performance. Figure 2 illustrates the linear piezoelectric energy harvester, which is distinctively designed with two tip masses.

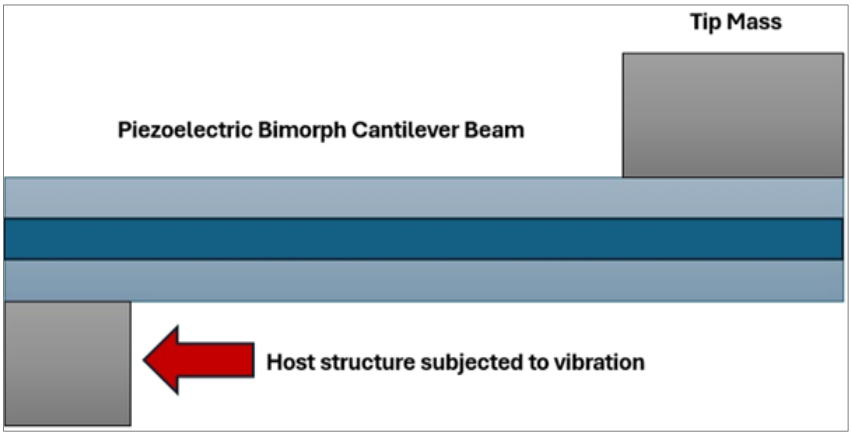

Figure 2. Linear Piezoelectric Energy Harvester Model

2.2. Non-Linear Model

In the construction of the nonlinear model, two permanent magnets were strategically positioned at an identical elevation, playing a dual role in the system's architecture. Not only do these magnets form an integral part of the model's structure, but they also function as the proof mass, essential for the device's operation. This innovative arrangement introduces magnetic forces into the system, creating a nonlinearity that significantly impacts the harvester's behavior and efficiency. Transitioning this model to a linear framework is straightforward yet profound in its implications. By replacing the permanent magnets with a non-magnetic proof mass, the system simplifies, eliminating the magnetic interactions that contribute to its nonlinear characteristics. The introduction of two magnets generates a fluctuating magnetic field through their interaction, influencing the mechanical response of the harvester and resulting in nonlinear behavior

The substitution of proof masses with permanent magnets allows for the introduction of a magnetic repulsion force, denoted as F_m. The nonlinear force can be expressed as follows:

$$F_m = \mu x(t) + \lambda x^3(t) \tag{6}$$

The term $\mu x(t)$ represents the linear stiffness component, where μ being the linear stiffness coefficient and $x(t)$ signifies the displacement. $\lambda x^3(t)$ denotes the nonlinear stiffness component, with λ representing the coefficient of cubic stiffness and $x^3(t)$ denoting the cubic term of displacement [52].

Hence, Equation 1 can be re-written once the piezoelectric energy harvester is magnetically coupled by using permanent magnets [52],

$$M\ddot{x}(t) + C\dot{x}(t) + Kx(t) - \theta v(t) = F(t) + F_m \tag{7}$$

The two magnets are positioned at the same elevation, maintaining a minimum gap of "d" between them, which is systematically varied to analyse its impact on the system. A repulsive magnetic orientation is beneficial for energy harvesting applications. The induced bistable behavior and increased bandwidth associated with repulsive forces can lead to improved voltage and power output in piezoelectric cantilever systems [53]. In theory, the repulsive force magnitude between the magnets diminishes as the distance between them increases. Both magnets are aligned with their same poles facing each other, as depicted in Figure 3, facilitating the generation of repulsive forces between them.

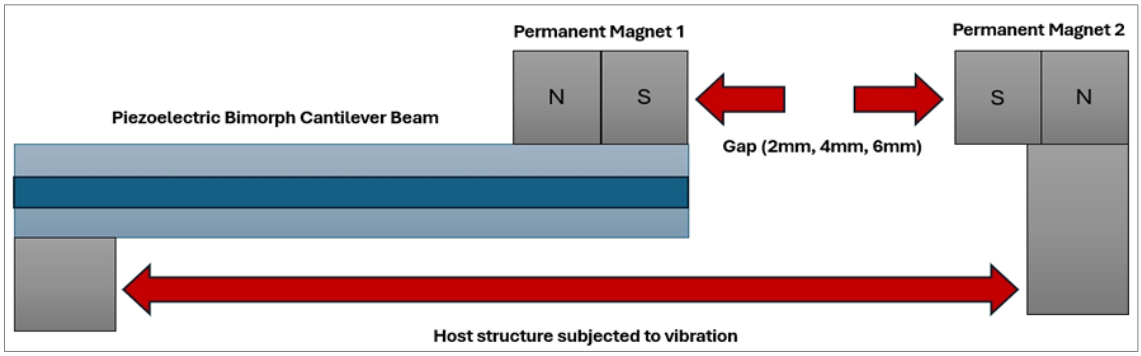

Figure 3. Nonlinear Piezoelectric Energy Harvester Model

Upon repulsion between the coupled magnets, two distinct vertical elevations are observed. This dual elevation, represented as "h" in Figure 4, suggests the likelihood of multiple resonances in the output predicted by the system. The inversion of the magnet along the vertical axis results in Equation 8, where F_{mv} represents the vertical repulsive force [22].

$$F_{mv} \cong F_m x/d - F_m x^3/2d^3 \tag{8}$$

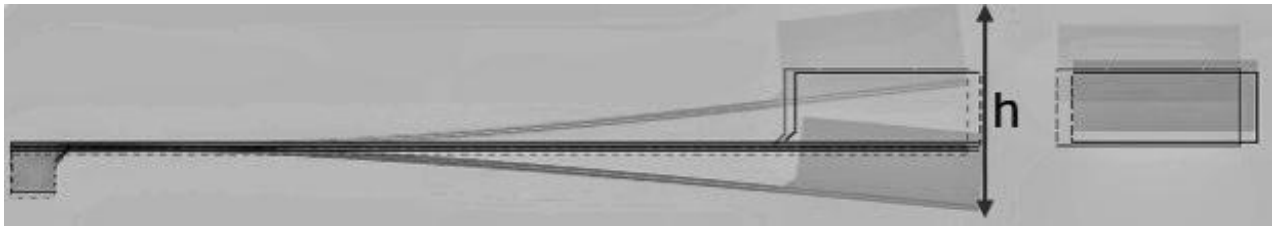

Figure 4. The flip of the beam

The resonant frequency of both the linear and nonlinear models can be described by Equation 9, with f_r representing the resonant frequency [54].

$$f_r = \frac{v_n'^2}{2\pi}\frac{0.001}{L^2}\sqrt{\frac{K_{tot}}{m_{eff}}} \tag{9}$$

In Equation 9, $v_n'^2 = v_n\sqrt{\frac{0.236}{3}}$, where v_n represents the eigenvalue with a value of 1.875. Here, L denotes the length of the beam, K_{tot} signifies the total stiffness of the system. K_{tot} can be calculated using Equation 10, with m_{eff} representing the effective mass of the system [54].

$$K = \frac{3EI}{L^3} \tag{10}$$

In Equation 10, E denotes the Young's Modulus of the material, and I represents the moment of inertia, which can be determined using Equation 11, where b for the width and h is represents the height of the geometry [54].

$$I = \frac{b \times h^3}{12} \tag{11}$$

3. Simulation Model

A two-dimensional finite element model was developed to analyze both linear and nonlinear PEH systems. Two distinct models were constructed to capture their unique physical behaviors, while ensuring uniform geometrical parameters across both configurations. This consistency allowed differences in performance to be attributed directly to the system physics rather than design variations. The main differences between the models were introduced through the proof mass material and the frequency ranges considered. The key parameters are summarized in Table 1, where E denotes the Young's modulus of the material and I represents the moment of inertia, defined in Equation 11 with b as width and h as height.

Table 1. Simulation parameters

Parameters	Values
Length of the tip mass	4 mm
Height of the tip mass	1.7 mm
Length of cantilever beam	21 mm
Height of the cantilever beam	0.16 mm
Thickness of piezoelectric layer	0.12 mm (0.06/layers)
Thickness of substrate layer	0.04 mm
Piezoelectric Material	Lead Zirconate Titanate-5A (PZT-5A)
Substrate Material	Aluminium
Proof Mass Material	Aluminium
Permanent Magnet Material	Neodymium Iron Boron (NdFeB)
Frequency Range (Linear)	0-300 Hz
Frequency Range (Non-Linear)	0-1000 Hz
Gap Between Magnets	2, 4, 6 (mm)

After the model's geometry was established, specific materials were allocated to each part of the model. FEA analysis boasts an extensive array of pre-defined materials, covering a wide range of material properties to suit various simulation needs. For this particular project, the necessary materials were already accessible within the FEA analysis, eliminating the need for custom additions. The characteristics of these materials are thoroughly documented in Table 2.

Table 2. Material properties

Material	Young's Modulus (GPa)	Density (kg/m^3)	Poisson's ration
Lead Zirconate Titanate-5A	66	7750	0.31
Aluminium	70	2700	0.33
Neodymium Iron Boron	160	7500	0.30

Boundary conditions were then applied by fixing endpoints, grounding surfaces, and defining terminal charges. The frequency range was adjusted according to study requirements, and output expressions were included to visualize voltage and electrical response. For the nonlinear configuration, additional physical processes were introduced through the Magnetic Fields physics module. Two identical mass blocks, defined as Magnet 1 and Magnet 2, were configured with opposite poles to generate repulsive forces, thereby introducing magnetic nonlinearity.

Finally, materials were assigned to each component of the model using COMSOL's built-in library of predefined properties. Since all required materials were readily available, no custom additions were necessary. The corresponding material characteristics are provided in Table 2.

3.1. Validation of Results with FEA Analysis

Utilizing materials, the constitutive relation of the B-H curve was extracted from the material to determine H_s, H_c and $W'_{m.}$ For materials not sourced from the library and defined by the user, these terms can also be specified accordingly.

The linear model's validation process involves a direct comparison with outcomes derived from two well-established finite element analysis (FEA) models, specifically referenced in the literature as [50, 55]. This comparison is crucial for verifying the accuracy and reliability of the linear model, ensuring its alignment with accepted standards within the scientific community. The comparison reveals that, when subjected to analogous simulation conditions, the linear model and the referenced FEA models yield indistinguishable results, affirming the linear model's validity and its adherence to expected physical principles.

In contrast, the assessment of the nonlinear model takes a different approach by comparing its simulated outcomes with real-world experimental data, cited as [22]. This comparison is instrumental in understanding how well the nonlinear model replicates complex real-life phenomena, particularly those involving nonlinear dynamics that are challenging to model accurately. Despite the inherent challenges in matching simulation with experimentation, especially due to the nonlinear model's sensitivity to specific conditions and parameters, the analysis unveils that both the simulation and experimental findings, although not identical, share similar scales of outcome. This similarity in magnitude suggests that the nonlinear model captures the essential dynamics of the system with a reasonable degree of accuracy, offering valuable insights into the behavior of nonlinear systems under various conditions.

4. Results and Discussion

4.1. Structural Analysis

The cantilever structure deformed at its first natural frequency of 70.5 Hz. Figure 5 illustrates the displacement of the cantilever beam along with its proof mass. As the second block mass remained fixed, no deformation or displacement was observed.

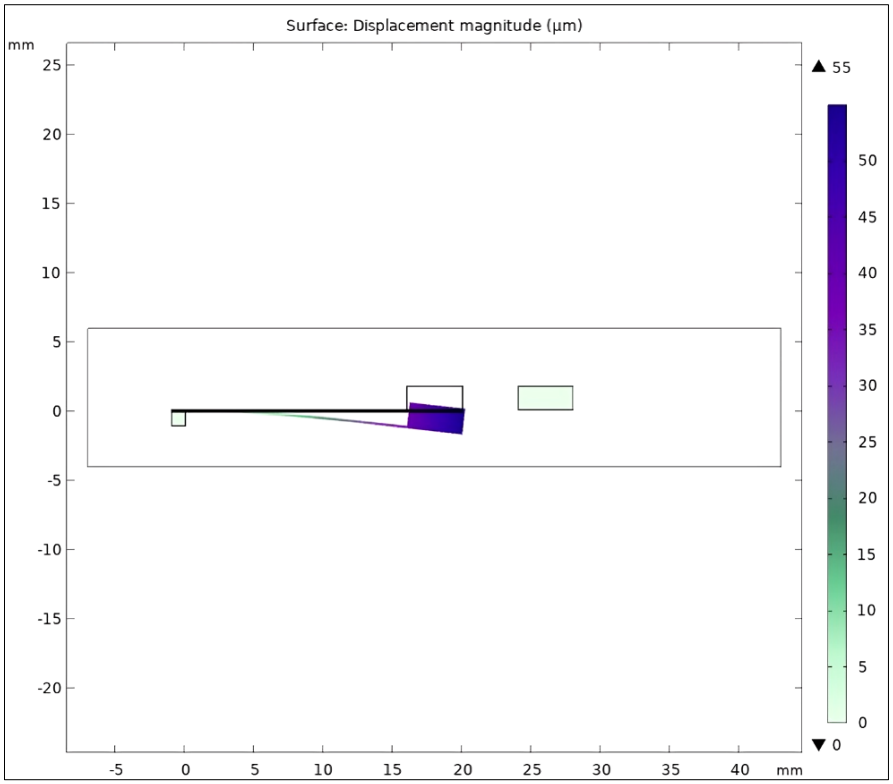

Figure 5. Mode shape of the model

The excitation force of the harvester consisted of its body load, which can be expressed as follows:

$$F_e = \rho_s . g . a \tag{12}$$

where, ρ_s denotes the density, g and a are the gravitational force and acceleration [55].

With the acceleration maintained at 1 ms^{-2}, minimal body load acted on the cantilever, resulting in a low magnitude of stress, as depicted in Figure 6.

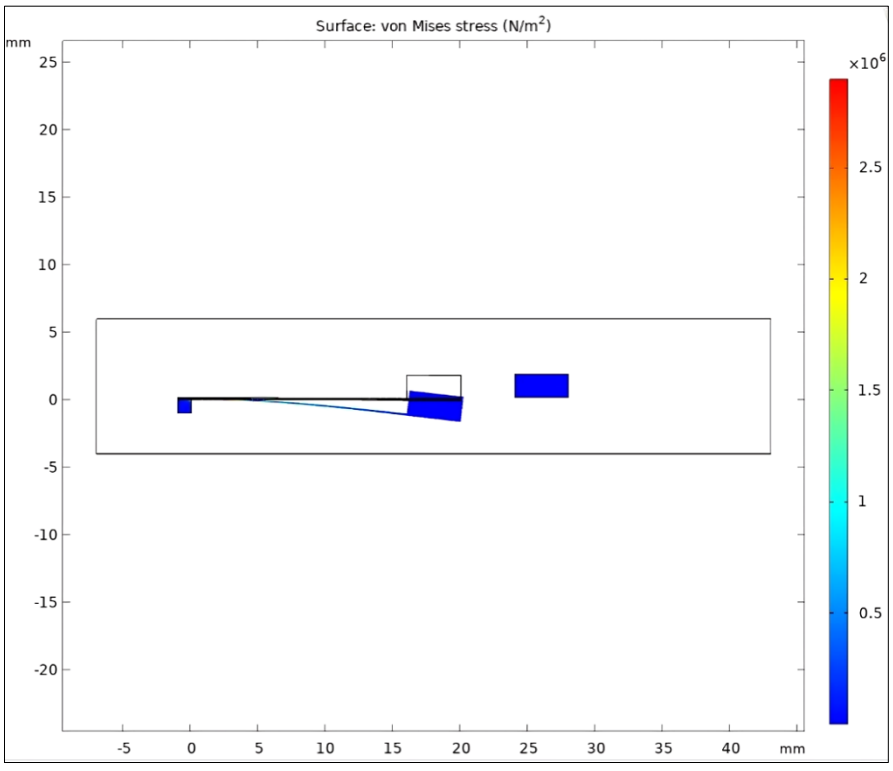

Figure 6. Stress distribution on the model

4.2. Voltage and Power Generation

4.2.1. Linear PEH

Figure 7(a) and (b) illustrate a detailed depiction of the performance of a linear PEH across a spectrum of vibration frequencies being subjected to a resistive load of 12 kΩ. It captures the dynamic behavior of the device, showing an initial increase in both voltage and power output as the frequency of vibrations escalates. This upward trend continues until reaching a distinct peak at approximately 111 Hz, a point where the voltage attains its highest value and the power output of 0.29mW. Following this peak, there is a noticeable decline in both voltage and power as the frequency progresses beyond the peak point. It showcases a characteristic frequency band within which these devices are most efficient at converting vibrational energy into electrical energy. The peak performance at around 111 Hz signifies the optimal operational frequency for this particular PEH model, beyond which its efficiency diminishes. This behavior underscores the importance of matching the resonant frequency of linear PEHs with the predominant frequency of environmental vibrations to maximize energy harvesting potential.

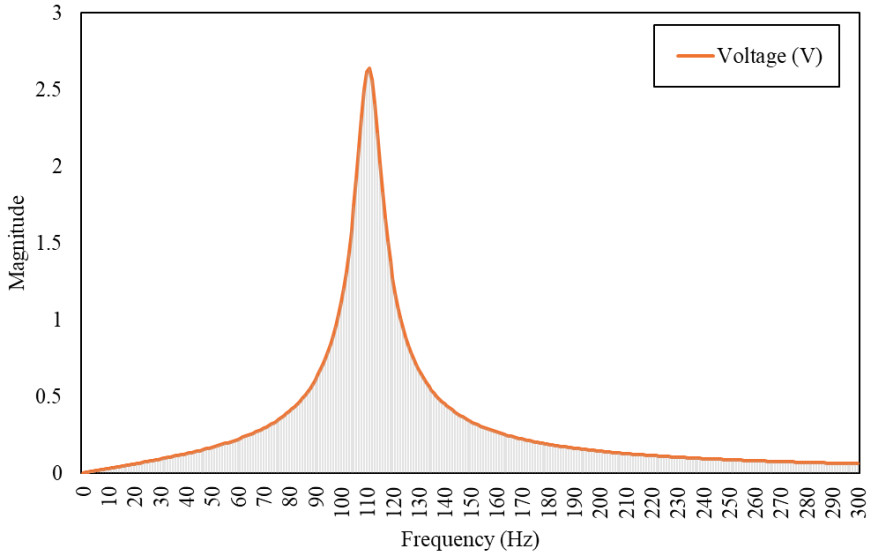

(a)

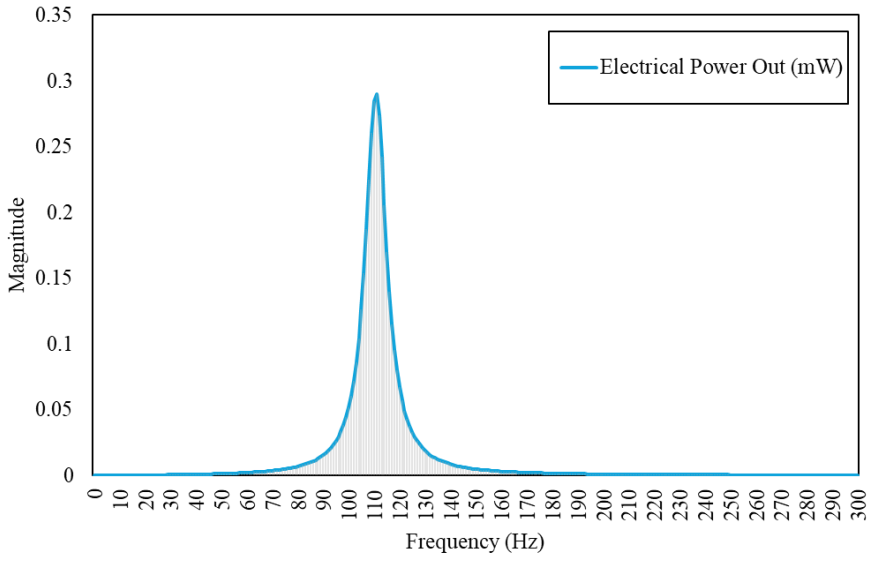

(b)

Figure 7. (a) Voltage response of the linear PEH (b) Electric power out response of the linear PEH

The peak voltage observed in the model aligns closely with the results from both analytical calculations and previously conducted FEA simulations concerning voltage generation. Table 3 showcases a comparison, relating the current model's voltage output against both the analytical predictions. According to the analytical model, the maximum voltage generation is estimated at 2.5 volts. Conversely, the outcomes from both FEA simulations consistently show a slightly higher peak voltage of 2.63 volts. This comparison not only validates the accuracy of the current model but also underscores the reliability of FEA simulations in predicting the performance of piezoelectric energy harvesting systems. Furthermore, this alignment between analytical and simulated data highlights the capabilities of FEA tools in

capturing the complex dynamics of piezoelectric systems, offering invaluable insights into optimizing device design for enhanced energy conversion efficiency.

Table 3. Voltage output comparison

Methods	Voltage (V)
Analytical	2.5
FEA (Current study)	2.63
FEA (Validated)	2.63

4.2.2. Non-Linear PEH

Figure 8 (a) and (b) illustrate the influence of varying gap distances between Magnet 1 and Magnet 2 on the voltage output and power generation of the nonlinear PEH across a broad frequency range. Three distinct magnet gaps were considered: 2 mm, 4 mm, and 6 mm. The results reveal that each configuration produces two prominent peaks in voltage output, a characteristic response of nonlinear harvesters arising from the additional restoring forces introduced by magnetic interactions. Unlike mode coupling, which results from the interaction of higher-order structural modes, the dual-peak behavior observed here originates from the nonlinear magnetic restoring forces. The repulsive magnets modify the system's potential energy landscape, creating a nonlinear stiffness profile that allows the system to respond at two resonance points. This phenomenon effectively broadens the operational bandwidth and enhances energy capture under varying excitation conditions.

In Figure 8(a), it is evident that a smaller gap distance (2 mm) yields higher voltage amplitudes, with the lower-frequency peak reaching approximately 7.8 V. This demonstrates the strong influence of magnetic proximity on system stiffness and electromechanical coupling, leading to superior energy harvesting potential. As the gap increases to 4 mm and then to 6 mm, a decline in voltage output is observed at both resonance peaks, with the lower-frequency peak showing the largest drop of approximately 1.56 V. These results confirm that closer magnet spacing intensifies magnetic repulsion, thereby increasing the nonlinear effect and boosting energy harvesting efficiency.

A similar trend is observed in Figure 8(b), where power generation also decreases as the magnet gap increases. Both resonance peaks exhibit reduced output with larger spacing, though the decline is more pronounced at the lower-frequency peak. At the 2 mm gap, the maximum power reaches approximately 2.55 mW, while the 6 mm gap results in a reduced peak power of about 1.63 mW. This reinforces the critical role of magnetic gap distance in dictating the operational performance of nonlinear PEHs. Overall, the results demonstrate that the two-peak response is a direct consequence of nonlinear magnetic interaction, and that minimizing the magnet gap significantly enhances both voltage and power outputs, thereby maximizing energy harvesting efficiency.

The observed reduction in performance at larger magnet gaps aligns with theoretical expectations: the magnetic force weakens with distance, diminishing its contribution to the nonlinear stiffness that drives energy conversion. This sensitivity to gap distance highlights the importance of precise magnetic alignment for optimizing performance. Furthermore, the close agreement between FEA predictions and experimentally validated data [22], as shown in Table 4, reinforces the reliability of the simulation approach in capturing the physical mechanisms at play.

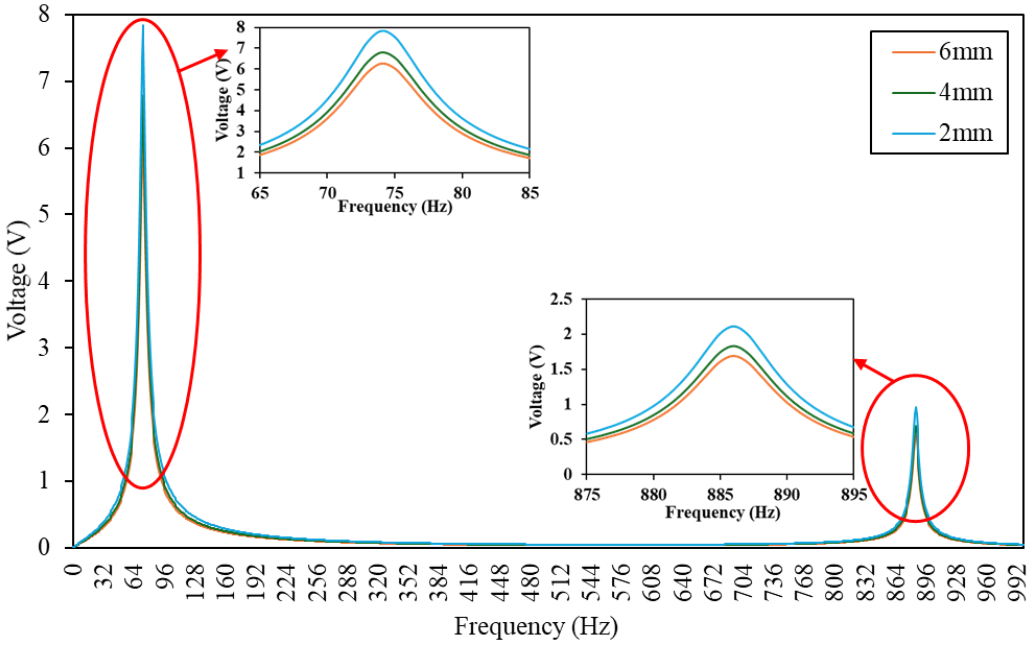

(a)

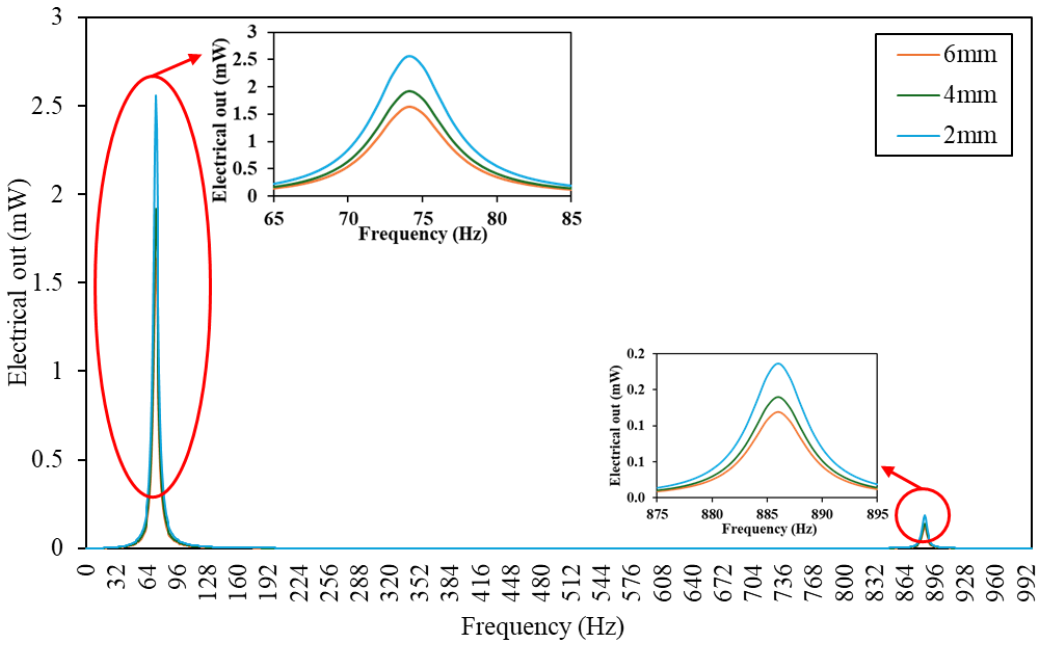

(b)

Figure 8. (a) Voltage output of nonlinear model (b) Power output of nonlinear model

Table 4. Voltage output comparison

Methods	Voltage (V)
FEA	7.8
Experimental	7.3

4.3. Performance Comparison

There was a clear distinction in the performance metrics of the two PEH models, with the nonlinear model outperforming the linear one in terms of voltage and power output. This difference is elaborately illustrated in Figures 9(a) and (b), showcasing the contrasting outcomes in voltage and power generation between the models. Notably, the nonlinear model achieved a peak voltage of 7.8 volts at a frequency of 74 Hz, significantly surpassing the linear model's maximum voltage of 2.63 volts at 111 Hz. This difference highlights a notable advantage in the nonlinear model's voltage production, marked by an abrupt rise in voltage at 72 Hz, which then quickly tapered off. On the other hand, the voltage trajectory of the linear model was characterized by a steady increment and decrement, showing a more uniform response pattern. This analogous pattern of growth and decline was also mirrored in the power generation profiles of both models, suggesting a similar dynamic in how power output fluctuates. The pronounced differences in peak performances and their respective paths underscore the unique efficiencies and operational behaviors of linear versus nonlinear models, with the nonlinear variant demonstrating enhanced potential for energy harvesting efficiency in certain conditions.

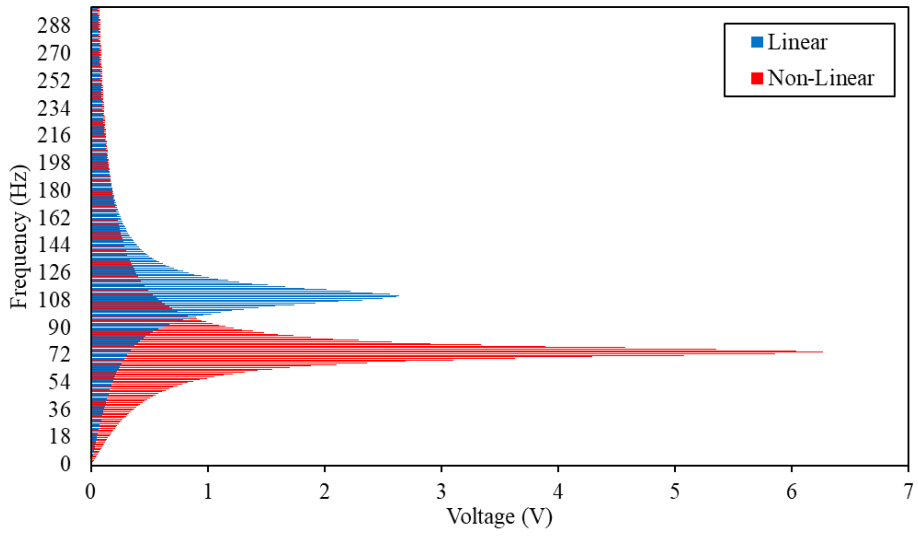

(a)

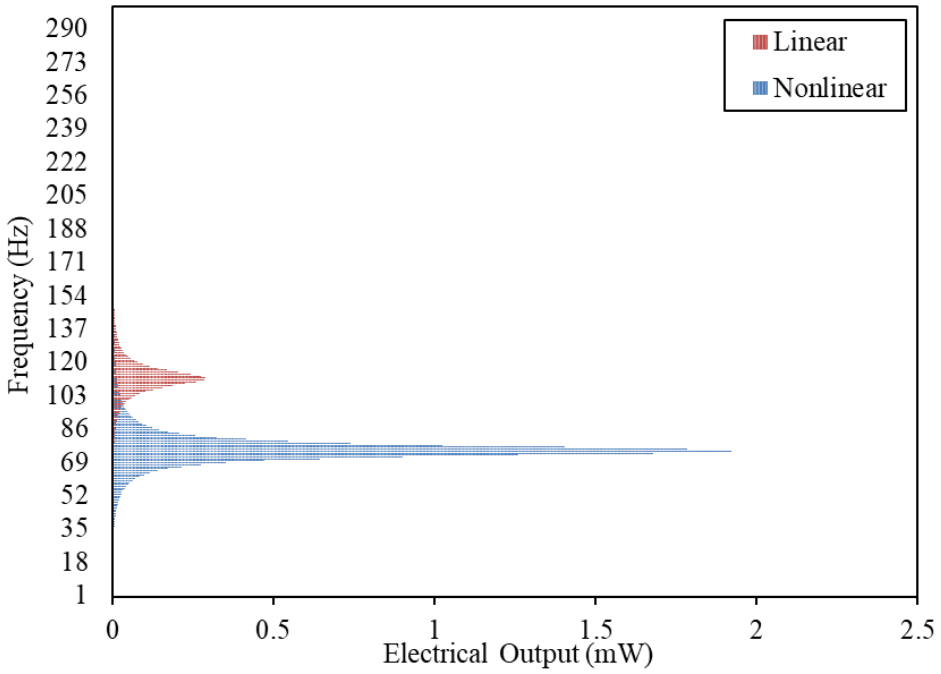

(b)

Figure 9. (a) Voltage comparison between linear and nonlinear PEH models (b) Power comparison between linear and nonlinear PEH models

Table 5 provides insight into the fluctuations of voltage and power output surrounding the peak frequencies of the models, with "N" indicating the peak frequency point. The data presented in Table 6 clearly illustrate the output dynamics of each model near their respective peaks.

For the linear model, the outputs subtly rise and fall within the range from N-3 to N+3, showing minor fluctuations in magnitude around the peak frequency. On the other hand, the nonlinear model demonstrates more dramatic changes, with significant spikes in both the ascent and descent of output values. Specifically, in the nonlinear model, there is a rapid increase in output magnitude leading up to the peak frequency (from N-3 to N), which is then followed by a marked decrease from the peak (N) down to N+3. This contrast underlines the distinct behavior of the nonlinear model in comparison to the steadier output pattern of the linear model, highlighting the variability and intensity of the nonlinear model's response to frequency changes. The pronounced spikes in the nonlinear model's output signify a critical operational characteristic, highlighting its ability to significantly outperform the linear model under optimal conditions.

Table 5. Graph comparison between linear and nonlinear PEH models

Frequency (Hz)	Linear (V)	Nonlinear (V)	Linear (mW)	Non-Linear (mW)
N-3	2.321167	5.368053	0.224492	0.901834
N-2	2.498193	6.349064	0.26004	1.261573
N-1	2.614053	7.32173	0.28472	1.677724
N	2.637611	7.835644	0.289875	1.921509
N+1	2.562996	7.551324	0.273706	1.784592
N+2	2.410438	6.69459	0.242092	1.402624
N+3	2.218447	5.719066	0.205063	1.023631

4.4. Resonant Frequency Comparison

The resonant frequency is theoretically influenced by various parameters of the materials employed in the system. Given that the overall mass of the system plays a crucial role in determining the resonant frequency, a system with a higher effective mass is expected to exhibit a lower resonant frequency. This principle is evident when comparing the nonlinear PEH model, which incorporates denser permanent magnets, to the linear PEH model that uses lighter aluminium for its proof mass. As a result, the nonlinear model, with its greater effective mass, naturally displays a resonant frequency that is lower than that of the linear model. This difference in resonant frequency between the models is clearly depicted in Figure 10.

Yet, experimental observations revealed that the actual resonant frequency was higher than those predicted by both analytical calculations and FEA simulations. These experimental findings were derived from a model operating under similar conditions as those described. The divergence between the experimental results and the FEA simulations can be attributed to minor differences in boundary conditions and system parameters. For instance, the analytical model for the nonlinear system predicted a resonant frequency of 76 Hz, while the FEA simulation identified a peak at 74 Hz. Similarly, for the linear model, analytical methods calculated a resonant frequency of 116 Hz, which contrasted with the 111 Hz peak observed in simulation results. This variation underscores the complexity of accurately predicting resonant frequencies and the impact of even slight discrepancies in system setup and conditions on these predictions. In physical setup, the magnetic field strength can fluctuate with varied distance. In simulation, the fluctuation may not be as precise. Moreover, there are additional parameters that are present at a physical set up, such as noise, external vibration and even heat. These conditions have not been considered hence the frequency response showcase a disparity against the experimental results.

The observation that mass differences contribute to the lower resonant frequency in the nonlinear model is consistent with theoretical expectations; however, the discrepancies between FEM and experimental results (76 Hz vs. 74 Hz vs. 111 Hz) warrant further elaboration. These differences arise from a combination of modeling assumptions and experimental uncertainties, which together influence the accuracy of frequency prediction.

A primary source of discrepancy lies in the material property assumptions used in FEM simulations. While the software relies on nominal values for constants such as Young's modulus, density, and piezoelectric coefficients, real materials often exhibit variability due to manufacturing tolerances, residual stresses, or compositional inhomogeneities. Even small deviations in these parameters can shift the natural frequency by several Hertz. Geometrical tolerances also play a role. Although the FEM model defines geometry precisely, experimental prototypes are subject to slight variations in beam thickness, width, or proof mass attachment. Because natural frequency scales with the stiffness-to-mass ratio, these dimensional inaccuracies can significantly alter resonance behavior.

Boundary conditions provide another explanation for the discrepancy. In FEM, the cantilever base is assumed to be perfectly clamped, yet in practice, fixtures may introduce compliance, damping, or micro-slippage, effectively reducing the system's stiffness and lowering the measured resonance frequency. This effect is particularly relevant in the nonlinear case, where additional uncertainties arise from modeling the magnetic interactions. The FEM model necessarily simplifies the magnetic field distribution, particularly at the edges of the magnets, whereas in experiments, even small misalignments or variations in magnet spacing can substantially alter the nonlinear restoring forces. This sensitivity explains why the nonlinear configuration shows the largest frequency deviation between simulation and experiment (111 Hz vs. ~76 Hz).

Finally, measurement limitations must also be considered. Experimental resonance identification depends on shaker excitation and data acquisition equipment, both of which are subject to environmental noise, finite frequency resolution during sweeps, and unmodeled damping effects. These factors can slightly shift the apparent resonance peaks compared with idealized FEM predictions.

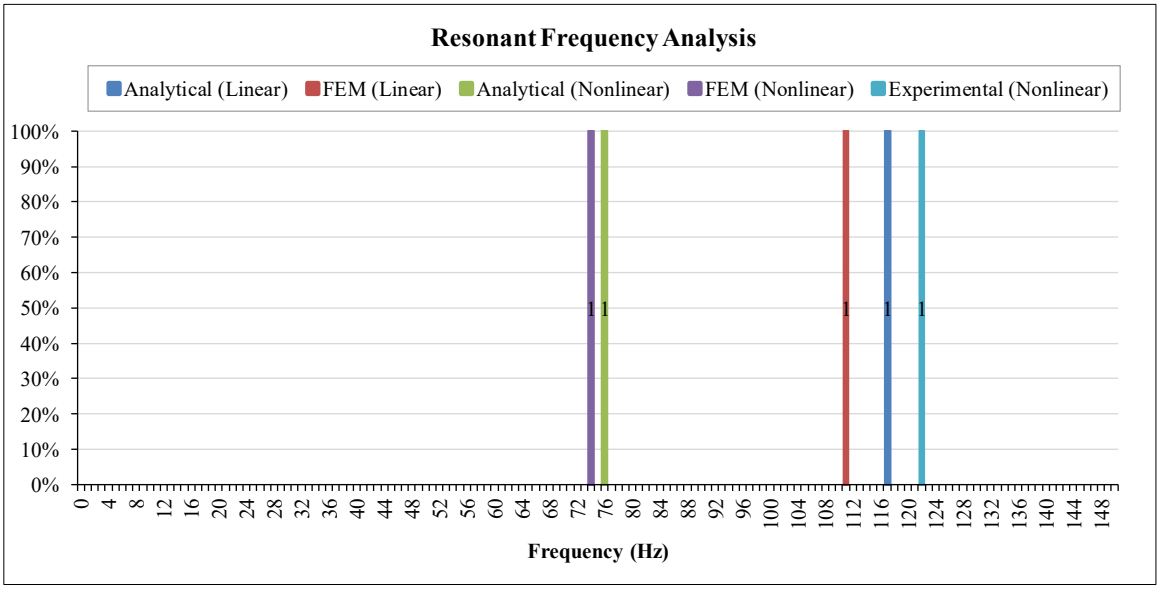

Figure 10. Resonant frequency analysis

4.5. Overall Comparison

On one hand, integrating permanent magnets and carefully tuning their alignment or gap distances provides a clear performance advantage: broader operational bandwidth, lower resonant frequency, and higher output power compared to conventional linear harvesters. This study shows this with the nonlinear model producing significantly higher voltage and power under identical conditions.

However, in real-world vibration environments, reliability becomes more challenging. Magnetic alignment and gap distance are highly sensitive to small variations. Any shift due to manufacturing tolerances, long-term material fatigue, or environmental disturbances (e.g., temperature fluctuations, mechanical shocks, or variable vibration amplitudes) can alter the nonlinear stiffness characteristics, thereby shifting resonance peaks or even degrading output. This added complexity increases the likelihood of performance inconsistencies in uncontrolled conditions.

In contrast, linear PEHs, although narrower in bandwidth, are structurally simpler and more predictable, making them inherently more reliable in long-term deployments. Thus, the trade-off is clear: nonlinear systems achieve superior energy harvesting performance but demand precise design, tuning, and potentially active control strategies to maintain stability and reliability in variable environments.

The reported results highlight a clear improvement in the nonlinear PEH compared to its linear counterpart, with the nonlinear design achieving up to 7.83 V and 1.92 mW versus 2.63 V and 0.29 mW in the linear configuration. In practical terms, these output levels are highly relevant for Internet of Things (IoT) applications and wireless sensor networks, where power demands typically range from a few hundred microwatts to a few milliwatts depending on duty cycle and data transmission frequency. For example, many low-power wireless sensors and Bluetooth Low Energy (BLE) devices operate in the range of 10 μW to 1 mW, particularly when supported by intermittent duty cycling and energy storage elements such as capacitors or thin-film batteries.

This implies that the nonlinear PEH developed in this study is capable of reliably powering intermittent wireless sensing tasks, such as environmental monitoring or structural health diagnostics, especially when paired with efficient power management circuits. The linear PEH, although more limited in power output, may still serve applications with ultra-low energy demands or where simplicity and robustness outweigh performance. Thus, the demonstrated performance not only validates the benefits of introducing magnetic nonlinearity but also underscores the feasibility of employing such designs in real-world IoT ecosystems.

The practical significance of the reported ~7.8 V and ~1.9 mW output can be better understood by examining its compatibility with real-world low-power devices. As summarized in Table 6, the generated power is sufficient to operate a broad class of IoT sensor nodes, structural health monitoring systems, and biomedical implants. For instance, wireless humidity or motion sensors typically consume less than 1 mW during transmission, while strain sensors used in SHM often require 0.5–2 mW depending on sampling frequency. Similarly, low-power biomedical devices, such as cardiac monitoring units or neural stimulators, operate within a comparable power range. These applications can therefore be directly supported by the proposed nonlinear PEH, particularly when combined with energy storage elements to buffer intermittent supply.

This mapping of harvested power to device requirements underscores the feasibility of deploying nonlinear PEHs in self-powered, energy-autonomous systems, thereby reducing reliance on batteries and extending device lifetime in IoT, SHM, and biomedical domains.

Table 6. Potential applications of the proposed nonlinear PEH compared with power requirements of representative low-power devices

Application Domain	Device Example	Typical Power Requirement	Compatibility with ~1.9 mW Output
IoT / Wireless Sensing	Wireless temperature or humidity sensor (Zigbee, BLE)	100 μW – 1 mW	Sufficient for intermittent sensing and transmission
	Motion/accelerometer sensor node	200 μW – 800 μW	Fully supported with energy storage
Structural Health Monitoring (SHM)	Wireless strain or vibration sensor	500 μW – 2 mW	Output meets requirements for periodic monitoring
Medical Implants	Cardiac/ECG monitoring sensor	500 μW – 1.5 mW	Compatible for continuous or duty-cycled operation
	Neural stimulator / biosensor	200 μW – 1 mW	Fully supported
Low-Power Electronics	BLE beacon / RFID tag	100 μW – 1 mW	Supported with energy buffering
	Wearable fitness tracker (sleep mode)	500 μW – 2 mW	Marginally sufficient, requires storage

5. Conclusion

This study evaluated the performance of piezoelectric energy harvesters by comparing linear and nonlinear configurations through analytical modeling and FEA simulations. The linear model produced a single resonance peak, achieving a maximum voltage of 2.63 V at 111 Hz and a power output of 0.29 mW, results that aligned closely with analytical predictions and previously validated simulations. In contrast, the nonlinear model, enhanced with permanent magnets, demonstrated markedly higher performance, generating two resonance peaks with the highest voltage of 7.83 V at 74 Hz and a maximum power output of 1.92 mW. These findings were consistent with experimental trends reported in the literature, despite minor deviations in resonant frequency.

The comparative analysis highlights the clear advantage of the nonlinear approach in significantly boosting voltage and power output, although this improvement comes with added system complexity and potentially higher fabrication costs. Importantly, the achieved output suggests that nonlinear PEHs hold strong potential for real-world applications, including powering low-power IoT devices, wireless sensor nodes for structural health monitoring, and selected biomedical implants in vibration-rich environments.

Building on these promising results, the next phase of this work will focus on experimental validation through physical prototyping. Fabrication and testing under controlled vibration conditions will provide critical confirmation of the simulation findings, while also addressing practical factors such as magnet alignment tolerances, damping effects, and long-term operational reliability. These steps are essential for bridging the gap between simulation and deployment, ultimately advancing nonlinear PEHs toward practical use in energy-autonomous electronic systems.

6. Declarations

6.1. Author Contributions

Conceptualization, F.H.S., L.W.T., and M.F.B.; methodology, F.H.S. and L.W.T.; software, F.H.S.; validation, F.H.S.; formal analysis, F.H.S., L.W.T., and M.F.B.; investigation, F.H.S.; resources, F.H.S. and L.W.T.; data curation, F.H.S.; writing—original draft preparation, F.H.S. and M.F.B.; writing—review and editing, L.W.T.; visualization, F.H.S. and L.W.T.; supervision, L.W.T.; project administration, L.W.T., Y.K.C., and M.N.E.E.; funding acquisition, L.W.T. All authors have read and agreed to the published version of the manuscript.

6.2. Data Availability Statement

The data presented in this study are available in the article.

6.3. Funding and Acknowledgments

This work was supported by the Ministry of Higher Education of Malaysia under the Fundamental Research Grant Scheme (FRGS/1/2020/TK0/MMU/03/13). The authors would also like to acknowledge the Faculty of Engineering and Technology, Multimedia University for the support given in conducting this research.

6.4. Institutional Review Board Statement

Not applicable.

6.5. Informed Consent Statement

Not applicable.

6.6. Declaration of Competing Interest

The authors declare that there are no conflicts of interest concerning the publication of this manuscript. Furthermore, all ethical considerations, including plagiarism, informed consent, misconduct, data fabrication and/or falsification, double publication and/or submission, and redundancies have been completely observed by the authors.

7. References

[1] Perez-Alfaro, I., Gil-Hernandez, D., Hernando, E., Quero, F., & Bernal, C. (2022). Electrical Response Analysis of a Piezoelectric Energy Harvester Power Source Based on Electromechanical Parameters. Electronics (Switzerland), 11(22), 3697. doi:10.3390/electronics11223697.

[2] De Marqui, C. (2016). Piezoelectric energy harvesting. Dynamics of Smart Systems and Structures: Concepts and Applications. John Wiley & Sons. doi:10.1007/978-3-319-29982-2_11.

[3] Katzir, S. (2006). The discovery of the piezoelectric effect. In The beginnings of piezoelectricity: a study in mundane physics (pp. 15-64). Dordrecht: Springer Netherlands. doi:10.1007/978-1-4020-4670-4_2.

[4] Tian, W., Ling, Z., Yu, W., & Shi, J. (2018). A review of MEMS scale piezoelectric energy harvester. Applied Sciences (Switzerland), 8(4), 645. doi:10.3390/app8040645.

[5] Mo, X., Zhou, H., Li, W., Xu, Z., Duan, J., Huang, L., Hu, B., & Zhou, J. (2019). Piezoelectrets for wearable energy harvesters and sensors. Nano Energy, 65, 104033. doi:10.1016/j.nanoen.2019.104033.

[6] Ali, A., Shaukat, H., Bibi, S., Altabey, W. A., Noori, M., & Kouritem, S. A. (2023). Recent progress in energy harvesting systems for wearable technology. Energy Strategy Reviews, 49, 101124. doi:10.1016/j.esr.2023.101124.

[7] Priya, S., & Inman, D. J. (Eds.). (2009). Energy Harvesting Technologies. Springer US. doi:10.1007/978-0-387-76464-1.

[8] Petrini, F., & Gkoumas, K. (2018). Piezoelectric energy harvesting from vortex shedding and galloping induced vibrations inside HVAC ducts. Energy and Buildings, 158, 371–383. doi:10.1016/j.enbuild.2017.09.099.

[9] Rosso, M., Kohtanen, E., Corigliano, A., Ardito, R., & Erturk, A. (2023). Nonlinear phenomena in magnetic plucking of piezoelectric vibration energy harvesters. Sensors and Actuators A: Physical, 362, 114667. doi:10.1016/j.sna.2023.114667.

[10] Syed, F. H., Thong, L. W., & Chan, Y. K. (2024). Effect of Repulsive Permanent Magnets on a Cantilever Beam-Based Piezoelectric Energy Harvester. 2024 Multimedia University Engineering Conference, MECON 2024, 1–6. doi:10.1109/MECON62796.2024.10776350.

[11] Ghandchi Tehrani, M., & Elliott, S. J. (2014). Extending the dynamic range of an energy harvester using nonlinear damping. Journal of Sound and Vibration, 333(3), 623–629. doi:10.1016/j.jsv.2013.09.035.

[12] Li, M., Yu, D., Li, Y., Liu, X., & Dai, F. (2023). Integrated a nonlinear energy sink and a piezoelectric energy harvester using simply-supported bi-stable piezoelectric composite laminate. International Journal of Non-Linear Mechanics, 156, 104464. doi:10.1016/j.ijnonlinmec.2023.104464.

[13] Liu, Q., Liu, H., & Zhang, J. (2025). Optimization of nonlinear energy sink using Euler-buckled beams combined with piezoelectric energy harvester. Mechanical Systems and Signal Processing, 223, 111812. doi:10.1016/j.ymssp.2024.111812.

[14] Hou, C., Shan, X., Dang, S., Du, X., Sui, G., & Xie, T. (2025). A magnetically excited broadband rotary piezoelectric energy harvester with nonlinear energy sink: Theoretical investigations and experimental Verifications. Mechanical Systems and Signal Processing, 224, 112085. doi:10.1016/j.ymssp.2024.112085.

[15] Li, T., & Lee, P. S. (2022). Piezoelectric Energy Harvesting Technology: From Materials, Structures, to Applications. Small Structures, 3(3). Portico. doi:10.1002/sstr.202100128.

[16] Al Anazi, A. A., Candra, O., Chammam, A., Marhoon, H. A., Ali, I. R., Al-Kharsan, I. H., Alayi, R., Ebazadeh, Y., & Aladdin, M. (2023). Modeling and investigating electric power output maximization for piezoelectric energy harvester. AIP Advances, 13(5). doi:10.1063/5.0141848.

[17] Chen, K., & Liao, W.-H. (2023). A nonlinear piezoelectric energy harvester with multiple auxetic unit cells. In Active and Passive Smart Structures and Integrated Systems XVII (Vol. 12483, p. 57). SPIE. doi:10.1117/12.2658624.

[18] Guo, C., & Luo, A. C. (2022). Nonlinear piezoelectric energy harvesting induced through the Duffing oscillator. Chaos: An Interdisciplinary Journal of Nonlinear Science, 32(12). doi:10.1063/5.0123609

[19] Man, D., Xu, G., Xu, H., & Xu, D. (2022). Parametric Analysis of Nonlinear Bi-Stable Piezoelectric Energy Harvester Based on Multi-Scale Method. Power Engineering and Engineering Thermophysics, 1(1), 19–32. doi:10.56578/peet010104.

[20] Pertin, O., Guha, K., Jakšić, O., Jakšić, Z., & Iannacci, J. (2022). Investigation of Nonlinear Piezoelectric Energy Harvester for Low-Frequency and Wideband Applications. Micromachines, 13(9), 1399. doi:10.3390/mi13091399.

[21] Ding, J., Deng, A., Zeng, Z., & Su, H. (2022). An innovative piezoelectric energy harvester inspired by a line tooth: design, dynamic model and broadband harvesting conditions. Smart Materials and Structures, 31(8), 085006. doi:10.1088/1361-665x/ac798d.

[22] Thong, L. W., Kok, S. L., & Ramlan, R. (2022). Parameter Optimization of Nonlinear Piezoelectric Energy Harvesting System for IoT Applications. International Journal of Advanced Computer Science and Applications, 13(5), 355–363. doi:10.14569/IJACSA.2022.0130542.

[23] Hegendörfer, A., Steinmann, P., & Mergheim, J. (2023). Numerical Optimization of a Nonlinear Nonideal Piezoelectric Energy Harvester Using Deep Learning. Journal of Low Power Electronics and Applications, 13(1), 8. doi:10.3390/jlpea13010008.

[24] Sheeraz, M. A., Malik, M. S., Rehman, K., Elahi, H., Butt, Z., Ahmad, I., Eugeni, M., & Gaudenzi, P. (2021). Numerical assessment and parametric optimization of a piezoelectric wind energy harvester for IoT-based applications. Energies, 14(9), 2498. doi:10.3390/en14092498.

[25] Mostafa, M. G., Motakabber, S. M. A., Ibrahimy, M. I., & Rahman, T. (2015). Parameter optimization for piezoelectric micro-energy harvesting system. Proceedings - 5th International Conference on Computer and Communication Engineering: Emerging Technologies via Comp-Unication Convergence, ICCCE 2014, 36–39. doi:10.1109/ICCCE.2014.23.

[26] Mane, P., Mossi, K., & Green, C. (2009). Optimizing energy harvesting parameters using response surface methodology. IEEE Transactions on Ultrasonics, Ferroelectrics, and Frequency Control, 56(3), 429–436. doi:10.1109/TUFFC.2009.1061.

[27] Rui, X., Li, Y., Liu, Y., Zheng, X., & Zeng, Z. (2018). Experimental study and parameter optimization of a magnetic coupled piezoelectric energy harvester. Applied Sciences (Switzerland), 8(12), 2609. doi:10.3390/app8122609.

[28] Patel, R., McWilliam, S., & Popov, A. A. (2014). Optimization of piezoelectric cantilever energy harvesters including non-linear effects. Smart Materials and Structures, 23(8), 85002. doi:10.1088/0964-1726/23/8/085002.

[29] Lin, Z., Yang, J., Zhao, J., Zhao, N., Liu, J., Wen, Y., & Li, P. (2016). Enhanced Broadband Vibration Energy Harvesting Using a Multimodal Nonlinear Magnetoelectric Converter. Journal of Electronic Materials, 45(7), 3554–3561. doi:10.1007/s11664-016-4531-4.

[30] Caetano, V. J., & Savi, M. A. (2025). Nonlinear Dynamics of a Piezoelectric Bistable Energy Harvester Using the Finite Element Method. Applied Sciences (Switzerland), 15(4). doi:10.3390/app15041990.

[31] Lin, Z., Li, H., Lv, S., Zhang, B., Wu, Z., & Yang, J. (2022). Magnetic Force-Assisted Nonlinear Three-Dimensional Wideband Energy Harvester Using Magnetostrictive/Piezoelectric Composite Transducers. Micromachines, 13(10). doi:10.3390/mi13101633.

[32] Wu, H., Tang, L., Avvari, P. V., Yang, Y., & Soh, C. K. (2013). Broadband energy harvesting using nonlinear 2-DOF configuration. In Active and Passive Smart Structures and Integrated Systems 2013 (Vol. 8688, p. 86880B). SPIE. doi:10.1117/12.2009100.

[33] Yang, J., Wen, Y., Li, P., Dai, X., & Li, M. (2010). A broadband vibration energy harvester using magnetoelectric transducer. In Proceedings of IEEE Sensors (pp. 1905–1909). IEEE. doi:10.1109/ICSENS.2010.5690026.

[34] Zhou, S., Cao, J., Erturk, A., & Lin, J. (2013). Enhanced broadband piezoelectric energy harvesting using rotatable magnets. Applied Physics Letters, 102(17). doi:10.1063/1.4803445.

[35] Lallart, M., Richard, C., Garbuio, L., Petit, L., & Guyomar, D. (2011). High efficiency, wide load bandwidth piezoelectric energy scavenging by a hybrid nonlinear approach. Sensors and Actuators, A: Physical, 165(2), 294–302. doi:10.1016/j.sna.2010.09.022.

[36] Pasharavesh, A., Moheimani, R., & Dalir, H. (2020). Performance analysis of an electromagnetically coupled piezoelectric energy scavenger. Energies, 13(4), 845. doi:10.3390/en13040845.

[37] Upadrashta, D., & Yang, Y. (2016). Nonlinear piezomagnetoelastic harvester array for broadband energy harvesting. Journal of Applied Physics, 120(5). doi:10.1063/1.4960442.

[38] Keshmiri, A., & Wu, N. (2018). A Wideband Piezoelectric Energy Harvester Design by Using Multiple Non-Uniform Bimorphs. Vibration, 1(1), 93–104. doi:10.3390/vibration1010008.

[39] Hajati, A., & Kim, S. G. (2011). Ultra-wide bandwidth piezoelectric energy harvesting. Applied Physics Letters, 99(8). doi:10.1063/1.3629551.

[40] Li, P., Gao, S., Zhou, X., Liu, H., & Shi, J. (2017). Analytical modeling, simulation and experimental study for nonlinear hybrid piezoelectric–electromagnetic energy harvesting from stochastic excitation. Microsystem Technologies, 23(12), 5281–5292. doi:10.1007/s00542-017-3329-5.

[41] Foupouapouognigni, O., Nono Dueyou Buckjohn, C., Siewe Siewe, M., & Tchawoua, C. (2018). Hybrid electromagnetic and piezoelectric vibration energy harvester with Gaussian white noise excitation. Physica A: Statistical Mechanics and Its Applications, 509, 346–360. doi:10.1016/j.physa.2018.06.026.

[42] Li, P., Gao, S., & Cai, H. (2015). Modeling and analysis of hybrid piezoelectric and electromagnetic energy harvesting from random vibrations. Microsystem Technologies, 21(2), 401–414. doi:10.1007/s00542-013-2030-6.

[43] Li, P., Gao, S., Cai, H., & Wu, L. (2016). Theoretical analysis and experimental study for nonlinear hybrid piezoelectric and electromagnetic energy harvester. Microsystem Technologies, 22(4), 727–739. doi:10.1007/s00542-015-2440-8.

[44] Li, Q., Wang, C., Liu, C., Li, Z., Liu, X., & He, L. (2025). Development Trend of Nonlinear Piezoelectric Energy Harvesters. Journal of Electronic Materials, 54(1), 1–23. doi:10.1007/s11664-024-11575-y.

[45] Zhou, S., Cao, J., & Lin, J. (2016). Theoretical analysis and experimental verification for improving energy harvesting performance of nonlinear monostable energy harvesters. Nonlinear Dynamics, 86(3), 1599–1611. doi:10.1007/s11071-016-2979-7.

[46] Kim, M., Hoegen, M., Dugundji, J., & Wardle, B. L. (2010). Modeling and experimental verification of proof mass effects on vibration energy harvester performance. Smart Materials and Structures, 19(4), 45023. doi:10.1088/0964-1726/19/4/045023.

[47] Erturk, A., & Inman, D. J. (2009). An experimentally validated bimorph cantilever model for piezoelectric energy harvesting from base excitations. Smart Materials and Structures, 18(2), 25009. doi:10.1088/0964-1726/18/2/025009.

[48] Abbasi, E. A., Allahverdizadeh, A., Jahangiri, R., & Dadashzadeh, B. (2017). Design and Analysis of a Piezoelectric Based AC Current Measuring Sensor. Article in International Journal of Mechanical & Mechatronics Engineering, 11(10), 1661–1666. doi:10.5281/zenodo.1132447.

[49] Kouritem, S. A., Al-Moghazy, M. A., Noori, M., & Altabey, W. A. (2022). Mass tuning technique for a broadband piezoelectric energy harvester array. Mechanical Systems and Signal Processing, 181, 109500. doi:10.1016/j.ymssp.2022.109500.

[50] Syed, F. H., Thong, L. W., & Chan, Y. K. (2023). Evaluation of Substrate Materials and Mass Structure on Piezoelectric Cantilever Based Energy Harvester. Journal of Engineering Science and Technology, 18(6), 3140–3154.

[51] Surmenev, R. A., Orlova, T., Chernozem, R. V., Ivanova, A. A., Bartasyte, A., Mathur, S., & Surmeneva, M. A. (2019). Hybrid lead-free polymer-based nanocomposites with improved piezoelectric response for biomedical energy-harvesting applications: A review. Nano Energy, 62, 475–506. doi:10.1016/j.nanoen.2019.04.090.

[52] Yang, Z., Zhou, S., Zu, J., & Inman, D. (2018). High-Performance Piezoelectric Energy Harvesters and Their Applications. Joule, 2(4), 642–697. doi:10.1016/j.joule.2018.03.011.

[53] Kumar, K., & Tyagi, A. (2025). Enhancing the Performance of Piezoelectric Vibration Energy Harvester Through Adjustments in the Geometric Configuration and the Volume of Additional Magnets. Journal of Vibration Engineering and Technologies, 13(1), 82. doi:10.1007/s42417-024-01615-6.

[54] Liu, H., Zhong, J., Lee, C., Lee, S. W., & Lin, L. (2018). A comprehensive review on piezoelectric energy harvesting technology: Materials, mechanisms, and applications. Applied Physics Reviews, 5(4). doi:10.1063/1.5074184.

[56] Jaafar, M. I., Rabah, H. M. M. M., Nordin, N. H. D., Muthalif, A. G. A., & Wahid, A. N. (2021). Voltage Generation in Piezoelectric Energy Harvesting with Magnet: FEA Simulation and Experimental Analysis. Journal of Science and Technology, 13(2), 17–24. doi:10.30880/jst.2021.13.02.003.